ADVANCED ELECTRONIC MATERIALS
www.advelectronicmat.de

Skin-Like Hybrid Integrated Circuits Conformal to Face for Continuous Respiratory Monitoring

*Ying Chen, Fei Liu, Bingwei Lu, Yingchao Zhang, and Xue Feng**

To perform wearable and continuous health monitoring, epidermal electronics for all kinds of sensing have been developed, yet neither organic nor inorganic materials-based epidermal devices are able to perform the functions like signal collection, processing, transmission, or power supply. Here, a strategy is reported to build skin-like hybrid integrated circuits (SHICs) with stretchable sensors and commercial chips for long-term respiratory monitoring. It can independently perform signal acquisition, processing, converting, and wireless transmission with carrying power supply. Thermal theory model is established to characterize the breathing air's interaction with the sensor, which helps in signal analysis. Respiratory monitoring on human body is tested in diverse daily activities including exercising, dining, drinking, and sleeping with a custom-developed phone application to record and display the respiratory signal. Results show that the SHIC is of high efficiency and accuracy to track the breath patterns continuously in both static and moving scenarios. Furthermore, the SHIC is a feasible and promising platform that can be extended with multiple sensors or actuators in individualized medical applications and physiological study.

Breathing is the process for air exchange between the human body and the environment. Being the basic physiological activity, breathing has been recognized to be intimately interactive with human mind and human body.[1] Breathing patterns can reflect both physical and mental status, for instance, rapid and shallow breathing indicates stress, panic, or fear,[2] and exhaled breath temperature rising marks the airway inflammation in asthma.[3–5] On the other hand, deliberate breath control can impact human body physically and mentally. Many health problems like stress, anxiety, COPD (chronic obstructive pulmonary disease), and PTSD (post-traumatic stress disorder) can be alleviated or benefited from breathing practice.[6–9] Thus, continuous breath monitoring with good accuracy is important and highly desired both in daily-life and clinical applications like sleep medicine and rehabilitation.

Dr. Y. Chen
Institute of Flexible Electronics Technology of THU
Jiaxing, Zhejiang 314000, China
Dr. F. Liu, Dr. B. W. Lu, Y. C. Zhang, Prof. X. Feng
AML, Department of Engineering Mechanics
Center for Flexible Electronics Technology
Tsinghua University
Beijing 100084, China
E-mail: fengxue@tsinghua.edu.cn
The ORCID identification number(s) for the author(s) of this article can be found under https://doi.org/10.1002/aelm.202000145.

DOI: 10.1002/aelm.202000145

Sleep apnea, known as the sleep disorder featured by breathing pauses during sleep, is a common and typical disease which may bring complications like daytime fatigue and increase the risk of high blood pressure, heart attack, stroke, type 2 diabetes, and liver problems as well as deprive the good rest of the sleep partners that requires continuous breath monitoring.[10] As obesity together with the health awareness both increase globally, continuous monitoring of breath is ever wanted with the diagnosis and individualized therapy of the sleep apnea. Polysomnography (PSG), a multi-parameter recorder, is currently used in sleep lab and contains respiratory, electroencephalograph (EEG), electrocardiograph (ECG), electromyography (EMG), eye movement and blood oxygen, and so on.[11] Yet, wearing the multiple wires and devices on the body, together with the first night effect will put impact on the sleeping quality even cause sleeplessness, making PSG unsuitable for sleep breath disorder screening in a more massive scale and earlier stage. Thus, wearable breath monitoring techniques are developed to solve this problem.[12–15]

The wearable breath monitoring can mainly be divided into two styles. Respiratory sensors measuring the air flow caused temperature, humidity, or pressure change in the nose and mouth place can be called the nose style, which are usually conducted with a mask acting as the carrier of the sensors or the enclosed space for the breath flow while being uncomfortable for the wearer.[16–29] Devices measuring the breath-induced deformation or impedance change of the chest or abdomen, called body style, are suffering from the noise caused by body movement.[30–34] Also there are commercialized wearable products like Spire claiming to be the breath pattern tracker. However, owing to the uncomfortable wearing, limited accuracy in case of body movement, the stone-like Spire, and bulky clinical machines cannot meet the requirement of long-term and real-time breath monitoring.

By integrating with human body intimately, flexible and stretchable bioelectronics have been developed to measure the physiological parameters, such as body temperature, blood oxygen, blood glucose, sweat, pulse and ECG, EEG, EMG, and so on.[35–43] Yet, most of them are reported as discrete devices, which lack the integrated counterpart for signal processing and transmission. Here, we propose a strategy to build skin-like hybrid integrated circuits (SHICs) with stretchable sensors

and commercial chips for long-term respiration monitoring. The strategy completes the burgeoning stretchable and flexible sensors with integrated chips-based circuits for information process. The measuring principle is to capture the temperature change of the inhaled and exhaled air (the temperature of the exhaled air is close to body temperature while that of the inhaled is near the environment temperature), which is the standard method introduced by the American Academy of Sleep Medicine (AASM). Since human face is featured with sensitiveness, dynamic facial expression as well as sweat secretion, this integrated device (SHIC) is delicately designed with respect to facial anatomy and kinematics facts. Theoretical model based on thermal analysis is built to help with signal interpretation. The performance of long-term wearing and monitoring are tested and demonstrated during all kinds of daily activities including resting, exercising, dining, drinking, and sleeping, with a custom-developed phone application to display and record the breathing signal. It turns out that SHIC is efficient in breathing patterns (including respiratory rate, amplitude, and inhale/exhale air temperature) tracking continuously in both static and moving occasions, and especially effective in sleep apnea detection. Thus, accurate breath information can be offered to doctors or psychologists as a reference in diagnosis and therapy assessment. Specifically, it is feasible and promising in clinical applications of sleep apnea syndrome. Moreover, the SHIC also works as a platform that is ready to incorporate other sensing elements like resistive volatile organic compounds sensors and humidity sensors to enrich the measuring parameters in the future.

To integrate flexible devices on the human faces, the following aspects need to be concerned. The complicated morphology and the dynamic deformation of the mouth make it difficult for flexible device's integration. Moreover, the abundant facial nerves around the nose require the device to be mechanically invisible and breathable to avoid allergies. **Figure 1**a schematically demonstrates wearing the SHIC on the face to monitor breathing. The SHIC mainly contains the temperature sensor and the flexible circuit. The temperature sensor placed below the nostril is stretchable and breathable to accommodate the mouth movement, while the flexible circuit is placed onto the nose ridge which is mainly composed of bones and cartilage. The serpentine-shaped anisotropic conductive film (ACF) cables are used to connect stretchable sensors with the circuits.

The final product of the SHIC is shown in Figure 1b, and the sensor's image is zoomed in on the right. The sensor is small, thin (50 μm thick), and light with a bending stiffness smaller than that of the skin. As shown in Figure 1c, the sensor whose fabrication process is demonstrated in Figure S1a in the Supporting Information, includes encapsulation based on semipermeable film (SF), sensor part made of gold and patterned substrate made of polyimide (PI). The SF, permeable for vapor and air, yet impermeable for liquids, makes the temperature sensor breathable to the human skin. And the patterned substrate enhances the tensile strength of the wires, so that the gold thin film together with the patterned substrate can be strong enough to buckle out of the plane to minimize the in-plane strain when the device is stretched or compressed. In Figure S1b in the Supporting Information, the sensor is convolved to a sticker with a radius of 0.3 mm to evidence its excellent flexibility and also can be conformal to undevelopable spherical surface (made of polydimethylsiloxane, PDMS) as shown in Figure S1c in the Supporting Information.

The flexible circuit in the SHIC is realized by integrating commercial chips onto the predefined flexible printed circuit board (FPCB) made of polyimide. To be specific, Figure 1d demonstrates the layout of the FPCB, and the block diagram illustrates how the circuit works in Figure 1e. This integrated circuit contains eight modules that are labeled in the diagram. Two resistive temperature sensors can be connected into the integrated circuit at the reserved interfaces. The resistance is measured by the voltage divider before converted by the analog to digital converter (ADC) and been processed in the microprogrammed control unit (MCU). The Bluetooth low energy system on chip (BLE SOC) is adopted to transmit the processed signal to the mobile phone via antenna. And the signal is displayed in the custom-developed mobile phone application (APP). The signal are plotted as two curves on the APP user interface, where the Bluetooth connecting and data recording can be controlled. Video S1 in the Supporting Information shows how the APP works. As for the power supply, the button-like lithium battery (3.7 V) is working as the energy source. And the battery protection module is used to keep the battery from abnormalities like overcharging, over-discharging, or sudden short-out. An E-switch is adopted to manually determine the SHIC's turn on or not. The battery converted module is added to lessen the output voltage of the battery from 3.7 to 3.3 V which is the working voltage of BLE SOC and the data collecting circuit. Besides, to measure the resistance accurately, we choose an independent ADC chip rather than built-in ADC in the MCU chip. The detailed circuit design can be found in Figure S2 in the Supporting Information as well as in the Experimental Section. To be more conformal with the nose, transfer printing methods for stretchable devices based on micro-structured stamp and dry adhesion, and soft substrate designs for flexible circuits are the potential solutions which we will try to apply in the future works.[44–51]

Here, we build a thermal model to predict the breath signal. Actually the device measures the heat transfer between the inhale/exhale flow and the stretchable sensor in forced convection as demonstrated in **Figure 2**a. Given the sensor is thin and small, during the heat transfer the inner thermal resistance can be neglected compared with that on the surface. Therefore, lumped parameter method can be used to theoretically predict and analyze the breathing signal. This assumption has been validated by overlapping two sensors to measure the same breath signal, and the results are shown in Figure 2b where S1 and S2 are the breath signal and AS1 and AS2 are the amplitude of each breath signal (defined as the peak to valley difference in each wave). Thus, the temperature of the sensor during the respiratory process is shown as Equation (1), where A, V, ρ, and c are the surface area, volume, density, and specific heat of the sensor, respectively, and h is the convective heat transfer coefficient. Details can be found in the Experimental Section

$$T = \left(\int_0^t \frac{A}{V\rho c} h(s) T_{\text{air}}(s) \mathrm{e}^{\int_0^s \frac{A}{V\rho c} h(r)\mathrm{d}r} \mathrm{d}s + T_0 \right) \mathrm{e}^{-\int_0^t \frac{A}{V\rho c} h(r)\mathrm{d}r} \tag{1}$$

Supposing the flow speed is sinusoidal and the flow temperature is a step function, the temperature of the sensor, i.e., the breathing signal's variation with respect to different flow speed,

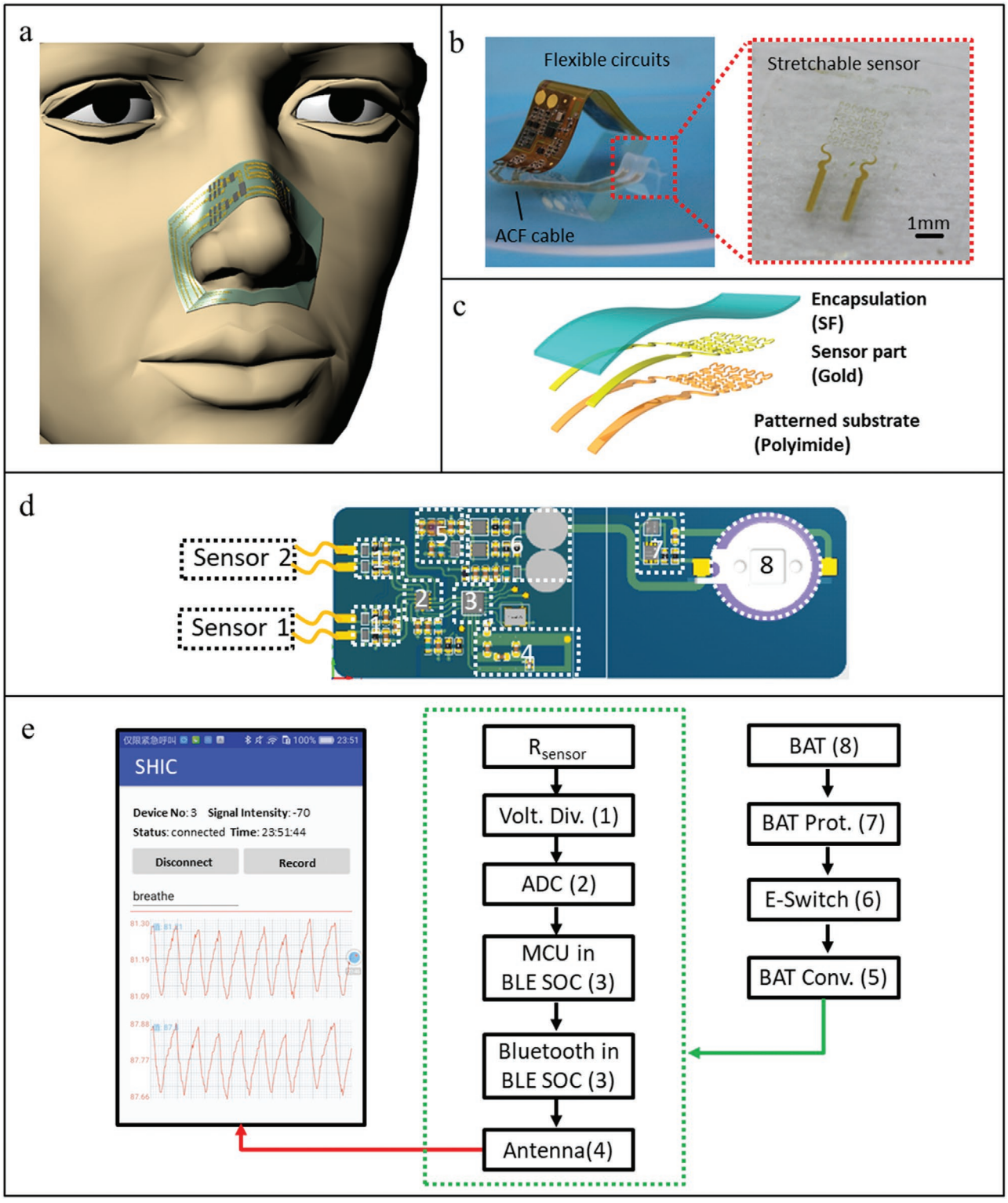

Figure 1. Demonstration and images of the SHIC for respiratory monitoring. a) Illustration of the SHIC wearing on the face to monitor breath. b) Photo of the SHIC, in which both flexible circuits and the stretchable sensors are bent, and the zoom-in image shows the stretchable sensor. c) The exploded view of the stretchable sensor. d) Layout of the flexible circuits. e) The block diagram to illustrate the circuit design.

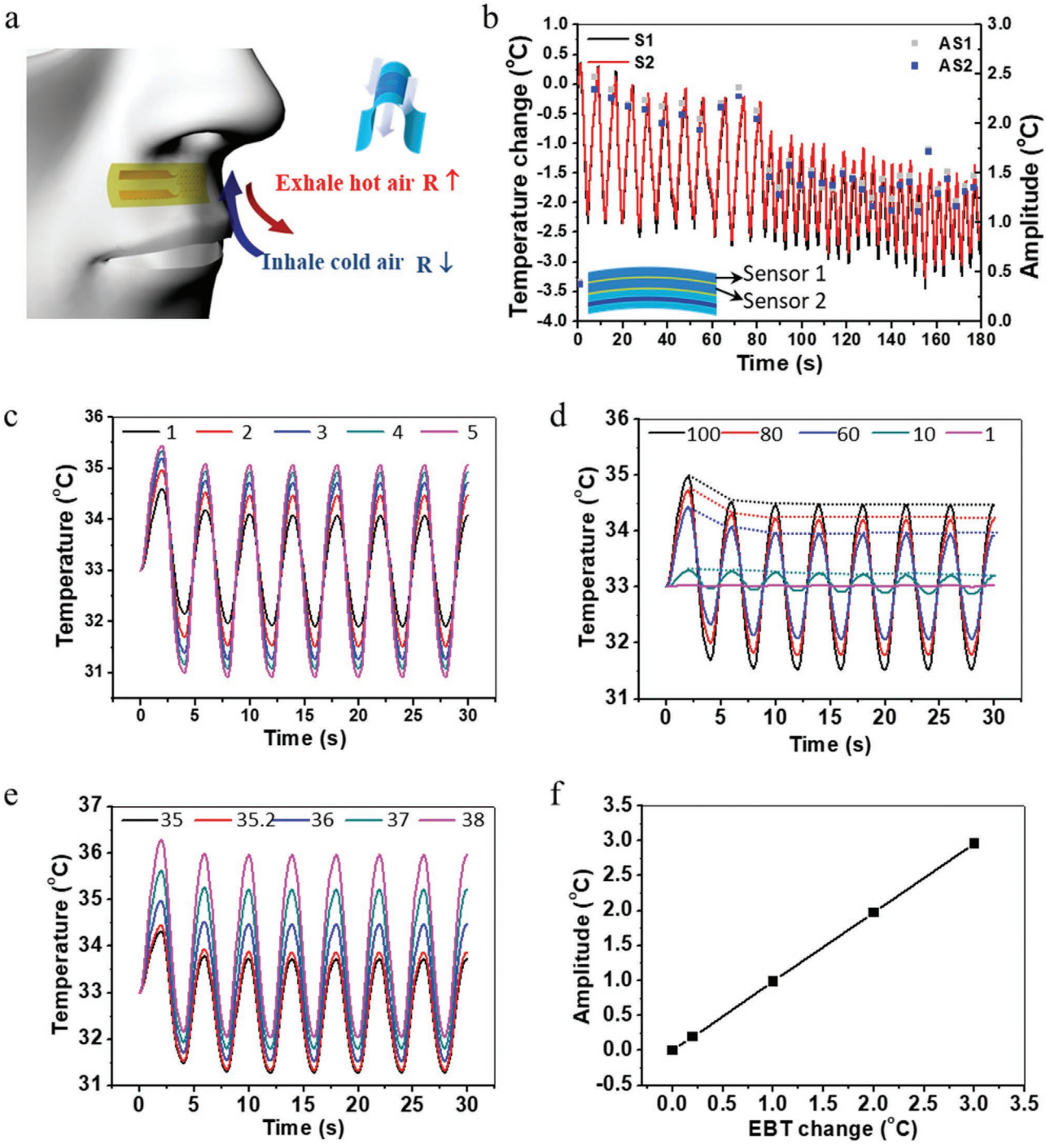

Figure 2. The theoretical analysis of the respiratory monitoring process. a) Illustration for measuring principle, and the inset is the illustration for air flowing from the buckled sensor. b) Dual-sensor measurement result shows that the temperature difference in the device is small enough to be ignored. c) The breathing signal predicted by Equation (1) with different flow speed (m s^{-1}). d) The breathing signal under different convective heat transfer coefficients from 1 to 100 W m^{-2} K^{f}. e) The breathing signal with different EBT (exhaled breath temperature) from 35 to 38 °C. f) The relationship of amplitude and the EBT change is linear.

convective heat transfer coefficient, exhaled breath temperature as well as the environment temperature have been analyzed. The main conclusions are: i) the flow speed variation exponentially changes the signal amplitude while the middle temperature (MT, the average value of the peak and valley) remains constant as shown in Figure 2c; ii) the convective heat transfer coefficient determines response time of the sensor as shown in Figure 2d, and the larger the coefficient the sooner, which requires the size of the sensor to be small; iii) the signal amplitude linearly increases with the EBT (exhaled breath temperature) as shown

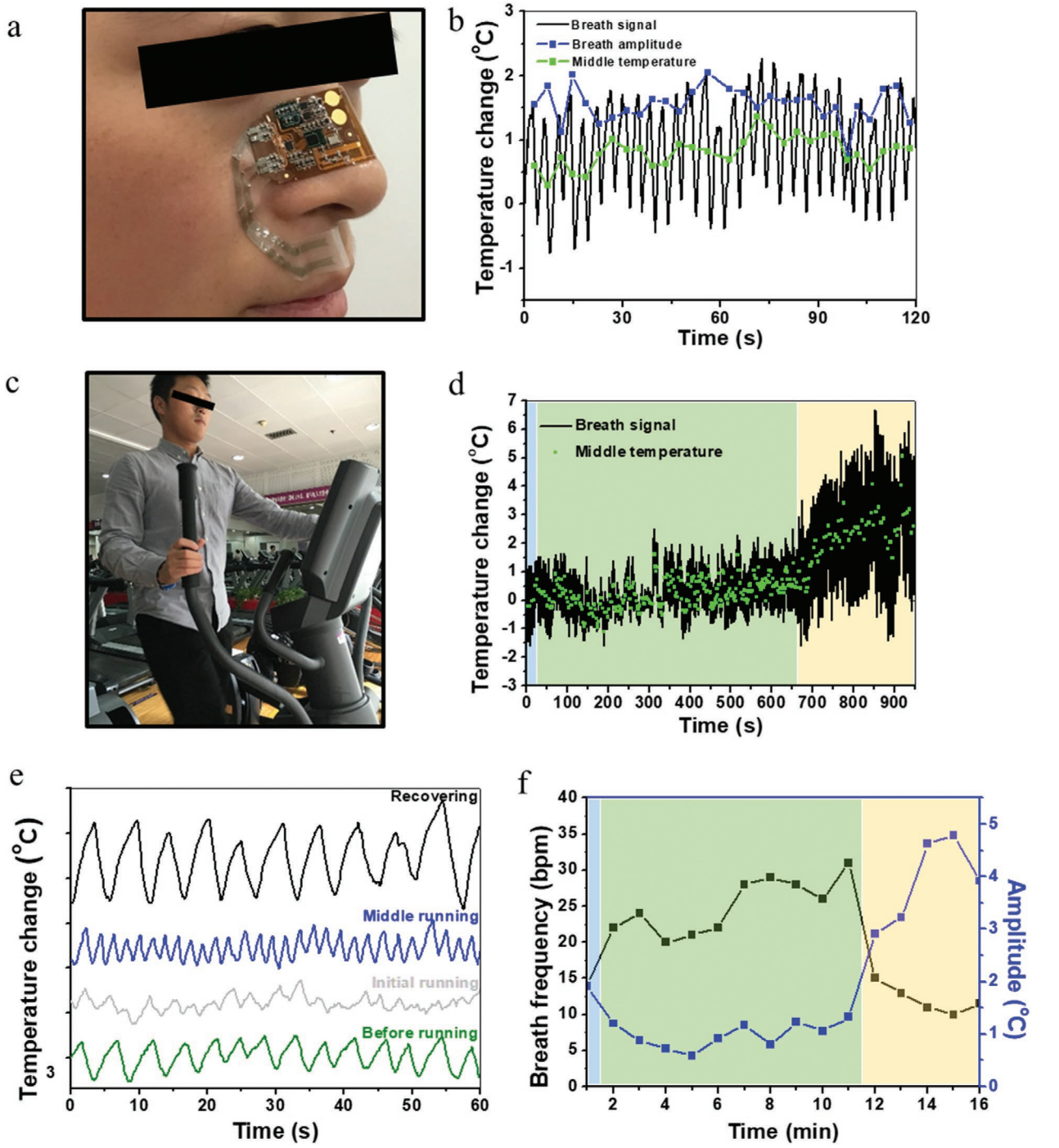

Figure 3. The performance of the device in respiratory monitoring during exercising. a) The photo for wearing the device on the face. b) The breath signal in resting state. c) The photo for wearing the device during exercising. d) The breathing signal in jogging. e) The segmented signal in jogging. f) The breath frequency and amplitude in jogging.

in Figure 2e,f; iv) IBT (inhaled breath temperature) is positively correlated with the MT and negatively with the amplitude, and the signal amplitude is linearly correlated with the difference of IBT and SBT (surface body temperature). This theory model shall be helpful during the breathing signal analysis by clarifying various factors' impacts on the breathing signal including EBT, SBT, IBT, and breathing frequency.

The long-term and wireless breath monitoring tests are conducted by wearing the SHIC to do a variety of daily activities including exercising, dining, and sleeping, and the signals are recorded and displayed by the custom-developed APP in real time. **Figure 3**a is the photo for SHIC wearing. Due to delicate design, the SHIC's wearing is comfortable for daily activities and physiological activities. Besides, its measured response and

recovery dynamics is shown in Figure S3 in the Supporting Information, where response time of 0.8 s and recovery time of 1.2 s can be read, which is faster than or comparable to that of the reported moisture sensor-based breath monitoring strategy (in which the response time is 2.2 s and recovery time is 1.05 s).[52] These times are much smaller than the human breathing period of 3–5 s (the natural human breathing rate is 12–18 bpm), indicating that the proposed device is sufficiently fast to monitor breathing signals. Figure 3b shows the breathing signal in stationary state. The black line is the raw data measured by the sensor, in which each wave indicates a single breath. With extremum search and Fourier transform, the amplitude (blue), middle temperature (green) of each breath, and the frequency in each minute can be obtained. Moreover, monitoring the breath in exercise has been conducted as shown in Figure 3c, when human body is severely dependent on this inhale and out-hale process to deliver oxygen in and carbon oxide out in the proper rhythm. Results show that the body movement will not be impacted by wearing the SHIC and the sweat can be evaporated by the micro-holes on the SF. The breath signal is shown in Figure 3d. The blue part indicates the preparing stage (1 min), the green is the exercising stage (10 min), and the yellow represents the recovering stage (5 min). Surely the rising MT (denoted by the green dots in Figure 3d) indicates the rising body temperature during the exercise. The breathing signal in each stage has been segmented in Figure 3e as four sections including before running, initial running, middle running, and recovering. As can be seen, the breath before running is regular with frequency of 14 bpm; in initial running section, the breath becomes irregular, especially in amplitude; then with conscious breath control and regulation, the breath becomes regular, shallow, and fast (with a higher frequency almost twice of that in preparing section); and in the recovering section, the breath is deep and slow. This breath evolvement is clear in the frequency and amplitude image shown in Figure 3f, where the frequency and amplitude change in an opposite direction in an exercise-and-recovering process. Quantitatively in this case, the signal amplitude is ≈50% lower in exercising section and ≈100% higher in recovering section than that in the stationary state. Hopefully with the SHIC device, studies on concern of breath and different exercise activities can be facilitated, accelerating the individualized and optimized breath techniques leading to better health.

Sleep disorder featured with breathing suspension requires continuous breathing monitoring during sleep. Oronasal thermal sensor is nominated by AASM (American Academy of Sleep Medicine) as the recommended method for sleep apnea detection in both adults and children. Here, SHIC adopts the same principle in breath monitoring, therefore it can be used in clinical screening or diagnosing. We have conducted breath monitoring in sleep with results shown in **Figure 4**a to testify the efficiency. The inset in Figure 4a shows the subject wearing the SHIC device in sleep, with no impact at any sleeping posture. The amplitude and frequency in Figure 4b characterize the breath more clearly, in which the green part indicates the awake situation and the blue part is falling asleep. The variation of amplitude and frequency suggests that the breath is shallower and faster in sleeping. And an unusually low frequency indicates possible apnea as emphasized in red circle, which is validated by the original signal within that minute as shown in the inset.

An algorithm based on fast Fourier transform is developed to capture the apnea behavior and its occurred time automatically. The preprocess of the data is to discrete the signal in time dimension with resolution of P1 and P2 (here P1 is 1 min and P2 is 10 min), then get the average signal amplitude (AA) and the average breath frequency by Fourier transform in every P1 and P2. Here the black line in Figure 4c is the raw data. The blue dot and square lines, respectively, represent the AA and average frequency in resolution of P1. And the blue and green straight lines, respectively, represent those in resolution of P2, in which the AA is 1.55 °C and the average frequency is 10.88 bpm. The time points in resolution P1, whose average frequency and the AA values are both below that in resolution P2 are marked as the suspicious points of apnea. To confirm the suspicious points, the raw data are tracked with the exact time coordinate in resolution P1 to further compare the breath pattern with the apnea definition in the instructional manual provided by AASM. Taking the raw data in Figure 4c as an example, after feeding them into this algorithm, minute 5 and 7 are marked as the apnea suspicious time. And it is testified by the raw data shown in Figure 4d, in which a 15 s /10 s breath-hold is existed in minute 5/7, respectively.

The SHIC's efficiency in different breathing manners including oral and nasal is also tested as shown in Figure 4e. The green parts indicate nasal breath when mouth is closed and the yellow represents oral breath when the mouth is open. Results show that both nasal and oral breathing can be detected by the SHIC. And the breath manner mainly affects the signal amplitude, since the heat convection caused by oral breath is weaker than that of nasal. The signal amplitude in oral breath is ≈50% smaller than that in nasal breath, apart from which, the necessary breath pattern including frequency, amplitude, and middle temperature can still be fully tracked by the SHIC. Thus, the performance and feasibility for the SHIC to monitor breath in sleep with any sleep posture or breathe manner is demonstrated and evidenced. However, It is noteworthy to mention that the proposed device will fail to operate if the ambient temperature is comparable to the body temperature, since no temperature gradient exists to drive the convective heat transfer.

Here, we propose a design and fabrication strategy for skin-like hybrid integrated circuits that can be integrated on the human face to measure the respiration for long term and wirelessly. This SHIC can be used to sense, measure, process, and transmit the breathing signal independently with its fully integrated sensors and commercial chips enabled flexible circuits. Custom-developed mobile phone APP has been built to display and record the breathing signal in real-time. The theory prediction is conducted by lumped parameter method to analyze the breathing signal. The capability of the device to work on the human body in all kinds of daily activities including resting, exercising, dining, drinking, and sleeping has been demonstrated. Breath frequency, amplitude, and exhaled air temperature can be obtained by data processing, which reveal the subject's physical status quantitatively and can be used to study the relationship of the breath and daily activities, especially in exercising. The abnormal behaviors of the breath, such as breath hold in sleep known as apnea, can be captured by the

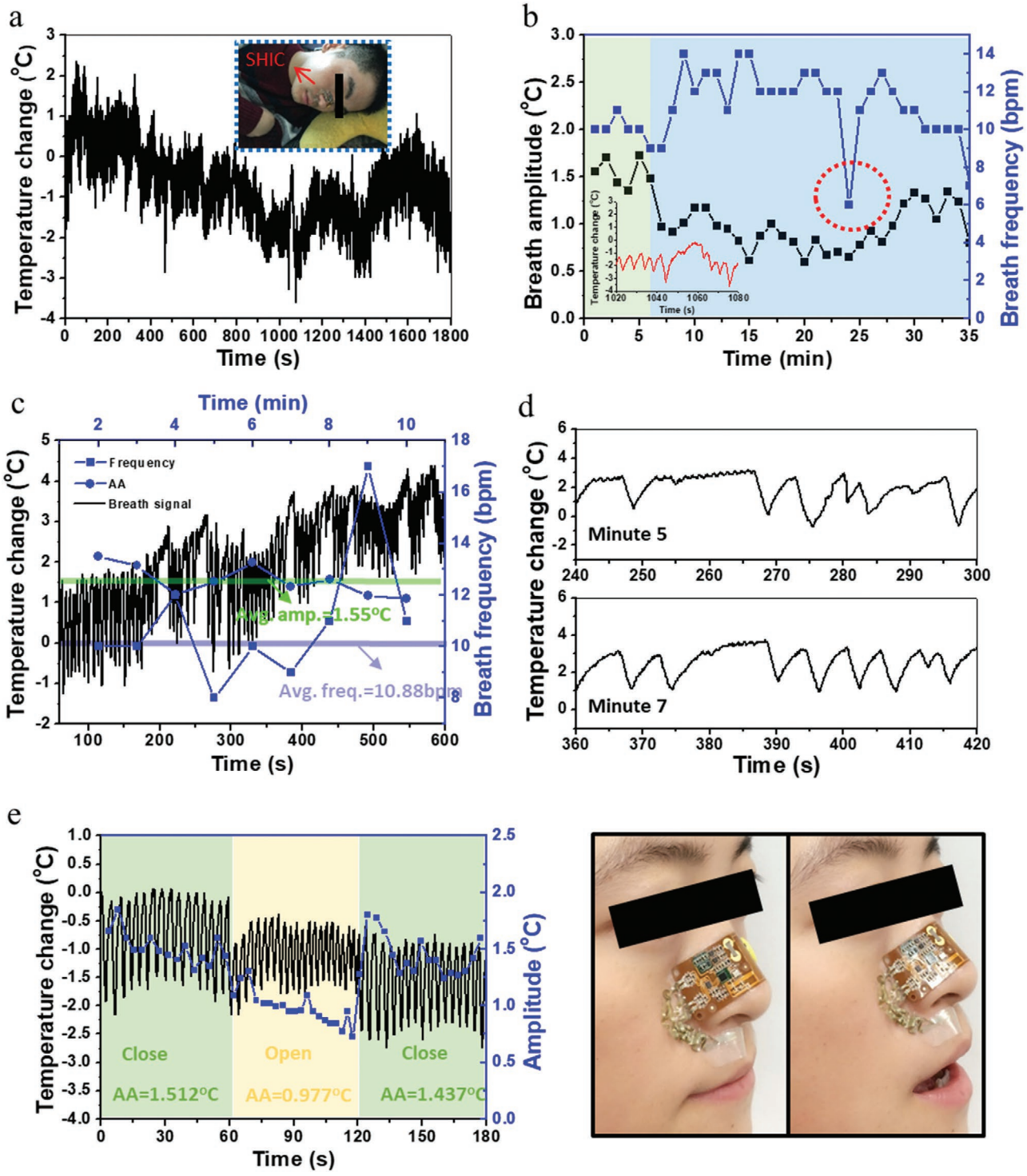

Figure 4. The respiratory monitoring and analysis in sleep. a) The raw data measured by the SHIC, and the inset shows the photo of the subject wearing the device during sleep. b) The amplitude and frequency of the data shown in (a) and the inset is the raw data containing the apnea. c) The demonstration of the data processing algorithm. d) The raw data in the apnea suspicious minute. e) The signal contrast in nasal and oral breathing and the corresponding photos are on the right.

SHIC. Hopefully this study can throw light on the development in system-level flexible and stretchable electronics and shorten their applications in healthcare and medical monitoring. To realize the commercialization of the SHICs, design of robust heterogenous interfaces, massive manufacturing of stretchable sensors, automated hybrid integration of the stretchable sensors, and flexible circuits are the main challenges. To tackle them, industrialization trials have been carried out.

Experimental Section

Circuit Design: The circuit design diagram is shown in Figure S2 in the Supporting Information. This circuit contained three core parts, i.e., the power management module, main control circuit with Bluetooth, and the ADC module. The power management module included battery, battery protector, E-switch, and the power converter. The battery denoted as BAT1 was a lithium battery with a voltage of 3.7 V. Battery protect chip U7 and dual MOSFET Q8 together formed the battery protector, which prevented the battery from the over-discharge, over-charge, short circuit, or other abnormity. Electrode TP11 and TP12, MOSFET Q2 and Q3 together formed the E-switch. When TP11 and TP12 were shorted by low resistance conductor (here a piece of conductive tape was used), Q3 turned on, so that the battery powered on the following circuits. The power converter was a voltage step-down regulator circuit, which decreased the original battery voltage to 3 V voltage. 3 V was the working voltage for the main control circuit and the ADC. The main control circuit was mainly dependent on a BLE SOC chip, which had built in a low power Bluetooth transceiver and a 32bit MCU with Cortex M0. This MCU had a built-in ADC with 1.2 V reference voltage and 10 bit resolution, which could monitor the voltage of the battery in real-time so as to estimate the battery level. The MCU could be programed by serial wire debug (SWD) interface. The main control circuit also included the antenna aided by several capacitors to transmit and receive signal wirelessly. ADC circuit was consisted of a 16 bit ADC chip U2 and a voltage divider (i.e., two sensors series connected to the constant resisters). The sensor's resistance could be obtained by measuring the sensor's voltage. Then the resistance was converted into digital signal in the ADC chip and sent to the MCU by SPI bus.

Fabrication of the Stretchable Temperature Sensor: The PDMS (Dow Corning Sylgard 184) with 10:1 ratio was spin-coated on the glass slide as the substrate for the device in micro-processing. The PI sheet (4–8 μm) was laminated onto the substrate before deposition of chromium 10 nm, and gold 150 nm by E-beam. Then the metal layers were patterned by photolithograph and wet etching, while another substrate was built by glass slide, scotch tape, and cured PDMS sheet. The PI sheet and patterned metal were transfer printed onto the new substrate to pattern the PI by RIE (150 W, 30 min), using the metal layer as mask. Then the ACF cable with the gold pad was connected by thermal pressure (170 °C, 10 min). Patterned metal/PI together with the PDMS sheet was transfer printed to the SF with the protective backing. After removing the PDMS sheet and backing layer, the final product was obtained. With the adhesive on the SF the sensor could be integrated onto any place of interest.

Theory Model for Respiratory Monitoring based on Lumped Parameter Method: On the assumption of uniform temperature distribution in the sensor, the heat transfer during the respiratory process could be characterized as

$$\frac{dT}{dt} = \frac{\dot{\Phi}}{\rho c} \tag{2}$$

in which T is the sensor's temperature, t is time, $\dot{\Phi}$ k is the generalized heat source, and ρ and c are the density and specific heat of the sensor, respectively. The heat transferred on the surface was converted into generalized heat source as

$$-\dot{\Phi}V = Ah(t)\left[T - T_{\text{air}}(t)\right] \tag{3}$$

in which A and V are the surface area and volume of the sensor, respectively, $h(t)$ is the convective heat transfer coefficient, and the $T_{\text{air}}(t)$ is the air temperature in the inhale/exhale process. Substituting (3) into (2) gave the differential equation

$$\frac{dT}{dt} + \frac{A}{V\rho c}h(t)\left[T - T_{\text{air}}(t)\right] = 0 \tag{4}$$

which together with the initial condition $T = T_0$ was able to describe the respiratory process theoretically. Solving this math problem gave the expression of the sensor's measuring temperature as

$$T = \left(\int_0^t \frac{A}{V\rho c}h(s)T_{\text{air}}(s)\mathrm{e}^{\int_0^s \frac{A}{V\rho c}h(r)\mathrm{d}r}\mathrm{d}s + T_0\right)\mathrm{e}^{-\int_0^t \frac{A}{V\rho c}h(r)\mathrm{d}r} \tag{5}$$

in which

$$h = 0.664\frac{\rho_{\text{air}}^{1/3}c_{\text{air}}^{1/3}\lambda_{\text{air}}^{2/3}}{\upsilon^{1/6}}\frac{\sqrt{|\nu|}}{\sqrt{l}} \tag{6}$$

with ρ_{air}, c_{air}, λ_{air}, υ, and ν denoting the density, specific heat, thermal conductivity, kinematic viscosity, and flow speed of the air and l denoting the characteristic length of the sensor. Here, the flow speed and temperature of the air were modeled as

$$\nu = \nu_{\text{peak}}\sin\left(\frac{2\pi t}{P}\right) \tag{7}$$

and

$$T_{\text{air}} = \begin{cases} T_{\text{exhale}} & nP \le t < (n + b_{\text{ex}})P \\ T_{\text{inhale}} & (n + b_{\text{ex}})P \le t < (n+1)P \end{cases} \quad n = 0,1,2,3,\ldots \tag{8}$$

respectively, in which ν_{peak} is the peak flow speed, P is the breath period, T_{exhale} is the EBT, T_{inhale} is the IBT, and b_{ex} is the ratio of the exhaled time to the whole breath period. The theoretical predictions and analysis of the breathing signal Equation (1) could be carried out by substituting (6)–(8) into (5).

Supporting Information

Supporting Information is available from the Wiley Online Library or from the author.

Acknowledgements

The authors express their sincere gratitude to Tsinghua Nanofabrication Technology Center for the assistance in the microfabrication. The authors gratefully acknowledge the support from the National Basic Research Program of China (grant no. 2015CB351904), National Natural Science Foundation of China (grant nos. 11625207, 11320101001, and 11902292).

Conflict of Interest

The authors declare no conflict of interest.

Keywords

breathing monitoring, hybrid integration, skin-like devices, sleep apnea, transfer printing

Received: February 8, 2020
Revised: April 9, 2020
Published online:

[1] W. E. Mehling, J. Wrubel, J. J. Daubenmier, C. J. Price, C. E. Kerr, T. Silow, V. Gopisetty, A. L. Stewart, *Philos. Ethics Humanit. Med.* **2011**, *6*, 6.
[2] A. Haag, S. Goronzy, P. Schaich, J. Williams, in *Emotion Recognition Using Bio-sensors: First Steps Towards an Automatic System* (Eds: E. André, L. Dybkjær, W. Minker, P. Heisterkamp), Springer, Berlin, Heidelberg **2004**, pp. 36–48.
[3] T. A. Popov, *Ann. Allergy, Asthma, Immunol.* **2011**, *106*, 451.
[4] G. García, M. Bergna, E. Uribe, A. Yañez, J. Soriano, *Int. J. Tuberc. Lung Dis.* **2013**, *17*, 969.
[5] P. Paredi, S. A. Kharitonov, P. J. Barnes, *Am J. Respir. Crit. Care Med.* **2002**, *165*, 181.
[6] E. M. Seppälä, J. B. Nitschke, D. L. Tudorascu, A. Hayes, M. R. Goldstein, D. T. Nguyen, D. Perlman, R. J. Davidson, *J. Trauma. Stress* **2014**, *27*, 397.
[7] S. Katiyar, S. Bihari, *Indian J. Allergy Asthma Immunol.* **2006**, *20*, 98.
[8] R. P. Brown, P. L. Gerbarg, *Ann. N. Y. Acad. Sci.* **2009**, *1172*, 54.
[9] S. Kriya, *J. Altern. Complementary Med.* **2005**, *11*, 189.
[10] C. Guilleminault, A. Tilkian, W. C. Dement, *Annu. Rev. Med.* **1976**, *27*, 465.
[11] N. J. Douglas, S. Thomas, M. A. Jan, *Lancet* **1992**, *339*, 347.
[12] M. Folke, L. Cernerud, M. Ekström, B. Hök, *Med. Biol. Eng. Comput.* **2003**, *41*, 377.
[13] Z. Wang, Z. Yang, T. Dong, *Sensors* **2017**, *17*, 341.
[14] F. Q. AL-Khalidi, R. Saatchi, D. Burke, H. Elphick, S. Tan, *Pediatr. Pulmonol.* **2011**, *46*, 523.
[15] Y. Liu, H. Wang, W. Zhao, M. Zhang, H. Qin, Y. Xie, *Sensors* **2018**, *18*, 645.
[16] B. M. Quandt, L. J. Scherer, L. F. Boesel, M. Wolf, G. L. Bona, R. M. Rossi, *Adv. Healthcare Mater.* **2015**, *4*, 330.
[17] P. Jiang, S. Zhao, R. Zhu, *Sensors* **2015**, *15*, 31738.
[18] Z. Lou, S. Chen, L. Wang, R. Shi, L. Li, K. Jiang, D. Chen, G. Shen, *Nano Energy* **2017**, *38*, 28.
[19] S. Malik, M. Ahmad, M. Punjiya, A. Sadeqi, M. S. Baghini, S. Sonkusale, presented at IEEE Sensors, New Delhi, India, Oct. **2018**.
[20] U. Mogera, A. A. Sagade, S. J. George, G. U. Kulkarni, *Sci. Rep.* **2015**, *4*, 4103.
[21] P.-G. Su, C.-F. Chang, *J. Taiwan Inst. Chem. Eng.* **2018**, *87*, 36.
[22] R. Cao, J. Wang, S. Zhao, W. Yang, Z. Yuan, Y. Yin, X. Du, N.-W. Li, X. Zhang, X. Li, *Nano Res.* **2018**, *11*, 3771.
[23] D. Shen, M. Xiao, G. Zou, L. Liu, W. W. Duley, Y. N. Zhou, *Adv. Mater.* **2018**, *30*, 1705925.
[24] H. Guo, C. Lan, Z. Zhou, P. Sun, D. Wei, C. Li, *Nanoscale* **2017**, *9*, 6246.
[25] F. Liao, Z. Zhu, Z. Yan, G. Yao, Z. Huang, M. Gao, T. Pan, Y. Zhang, Q. Li, X. Feng, *J. Breath Res.* **2017**, *11*, 036002.
[26] S. Kano, K. Kim, M. Fujii, *ACS Sens.* **2017**, *2*, 828.
[27] J. Park, Y. Lee, J. Hong, M. Ha, Y.-D. Jung, H. Lim, S. Y. Kim, H. Ko, *ACS Nano* **2014**, *8*, 4689.
[28] H. Xue, Q. Yang, D. Wang, W. Luo, W. Wang, M. Lin, D. Liang, Q. Luo, *Nano Energy* **2017**, *38*, 147.
[29] H. Jin, X. Tao, S. Dong, Y. Qin, L. Yu, J. Luo, M. J. Deen, *J. Micromech. Microeng.* **2017**, *27*, 115006.
[30] L. Guo, L. Berglin, U. Wiklund, H. Mattila, *Text. Res. J.* **2013**, *83*, 499.
[31] M. Li, H. Li, W. Zhong, Q. Zhao, D. Wang, *ACS Appl. Mater. Interfaces* **2014**, *6*, 1313.
[32] Z. Zhao, C. Yan, Z. Liu, X. Fu, L. M. Peng, Y. Hu, Z. Zheng, *Adv. Mater.* **2016**, *28*, 10267.
[33] O. Atalay, W. R. Kennon, E. Demirok, *IEEE Sens. J.* **2014**, *15*, 110.
[34] Y. Song, H. Chen, Z. Su, X. Chen, L. Miao, J. Zhang, X. Cheng, H. Zhang, *Small* **2017**, *13*, 1702091.
[35] F. Wang, D. Wu, P. Jin, Y. Zhang, Y. Yang, Y. Ma, A. Yang, J. Fu, X. Feng, *Sci. China Inf. Sci.* **2019**, *62*, 202402.
[36] Z. Han, H. Li, J. Xiao, H. Song, B. Li, S. Cai, Y. Chen, Y. Ma, X. Feng, *ACS Appl. Mater. Interfaces* **2019**, *11*, 33370.
[37] Y. Chen, S. Lu, S. Zhang, Y. Li, Z. Qu, Y. Chen, B. Lu, X. Wang, X. Feng, *Sci. Adv.* **2017**, *3*, e1701629.
[38] Z. Han, Z. Cheng, Y. Chen, B. Li, Z. Liang, H. Li, Y. Ma, X. Feng, *Nanoscale* **2019**, *11*, 5942.
[39] Y. Zhang, N. Zheng, Y. Cao, F. Wang, P. Wang, Y. Ma, B. Lu, G. Hou, Z. Fang, Z. Liang, *Sci. Adv.* **2019**, *5*, eaaw1066.
[40] S. Choi, H. Lee, R. Ghaffari, T. Hyeon, D. H. Kim, *Adv. Mater.* **2016**, *28*, 4203.
[41] J. Rogers, G. Malliaras, T. Someya, *Sci. Adv.* **2018**, *4*, eaav1889.
[42] Y. Ma, Y. Zhang, S. Cai, Z. Han, X. Liu, F. Wang, Y. Cao, Z. Wang, H. Li, Y. Chen, X. Feng, *Adv. Mater.* **2020**, *32*, e1902062.
[43] T. R. Ray, J. Choi, A. J. Bandodkar, S. Krishnan, P. Gutruf, L. Tian, R. Ghaffari, J. A. Rogers, *Chem. Rev.* **2019**, *119*, 5461.
[44] H. Luo, C. Wang, C. Linghu, K. Yu, C. Wang, J. Song, *Nat. Sci. Rev.* **2020**, *7*, 296.
[45] C. Linghu, S. Zhang, C. Wang, K. Yu, C. Li, Y. Zeng, H. Zhu, X. Jin, Z. You, J. Song, *Sci. Adv.* **2020**, *6*, eaay5120.
[46] C. Linghu, C. Wang, N. Cen, J. Wu, Z. Lai, J. Song, *Soft Matter* **2019**, *15*, 30.
[47] Z. Chen, C. Linghu, K. Yu, J. Zhu, H. Luo, C. Qian, Y. Chen, Y. Du, S. Zhang, J. Song, *ACS Appl. Mater. Interfaces* **2019**, *11*, 48412.
[48] M. Cai, S. Nie, Y. Du, C. Wang, J. Song, *ACS Appl. Mater. Interfaces* **2019**, *11*, 14340.
[49] J. Song, X. Feng, Y. Huang, *Nat. Sci. Rev.* **2016**, *3*, 128.
[50] F. Zhu, H. Xiao, H. Li, Y. Huang, Y. Ma, *J. Appl. Mech.* **2019**, *86*, 034501.
[51] A. Robinson, A. Aziz, Q. Liu, Z. Suo, S. P. Lacour, *J. Appl. Phys.* **2014**, *115*, 143511.
[52] U. Mogera, A. A. Sagade, S. J. George, G. U. Kulkarni, *Sci. Rep.* **2015**, *4*, 4103.

